Submitted to *Journal of the European Ceramic Society*, June 2019. Revised September 2019.

Manufacturing B_4C parts with Ti-Al intermetallics by aqueous colloidal processing

Cristina Ojalvo [a], Rodrigo Moreno [b], Fernando Guiberteau [a], Angel L. Ortiz [a,*]

[a] Departamento de Ingeniería Mecánica, Energética y de los Materiales, Universidad de Extremadura, 06006 Badajoz, Spain.

[b] Instituto de Cerámica y Vidrio, Consejo Superior de Investigaciones Científicas, Madrid 28049, Spain.

Abstract

The aqueous colloidal processing of submicrometre B_4C powder (~0.6 μm) with coarse Ti-Al powder (~40 μm) as sintering additive was investigated. Firstly, by measuring the zeta potential, pHs were identified that promote the individual colloidal stability of the B_4C and Ti-Al particles as well as their co-dispersion in water with two different deflocculants (one anionic and the other cationic). It was found that the anionic and cationic deflocculants shift the isoelectric points of B_4C and Ti-Al to more acidic and more basic pHs, respectively, making their co-dispersion possible at neutral pH. And secondly, by means of rheological studies, conditions were identified (sonication time, deflocculant type, and deflocculant content) that at quasi-neutral pH yield B_4C+Ti-Al shear-thinning concentrated suspensions (30 vol.% total solids) with low viscosity and small hysteresis loop. Interestingly, those deflocculated with the cationic polyelectrolyte had better rheological behaviour, being also less viscous and almost non-thixotropic. These suspensions were freeze-dried, obtaining powder mixtures that were compacted by conventional spark plasma sintering (SPS), and also slip-cast, obtaining robust

green pieces that were densified by pressureless SPS. The two B_4C composites thus obtained are superhard, with Vickers hardnesses greater than 30 GPa.

Keywords: B_4C; aqueous colloidal processing; aqueous ceramic suspensions; shaping; spark plasma sintering.

* Corresponding author:

Angel L. Ortiz
Phone: +34 924289600 Ext: 86726
Fax: +34 924289601
E-mail:**alortiz@unex.es**

1. Introduction

The great demand for ever harder ceramic parts for structural applications has led to soaring interest in the processing of advanced ceramics and composites based on B_4C, the third hardest compound known to man (after diamond and cubic BN) and the hardest compound synthesized routinely on a large scale (in tonnes) [1-3]. In addition, B_4C is not only superhard, but also ultra-lightweight and very refractory [1,3]. It excels in ballistic performance, and is indeed the reference material for the fabrication of personnel and vehicle armours [1-8]. It also stands out in wear resistance, and thus is a very appealing material for the manufacture of tribocomponents [1,2,9-15].

A common feature in these applications is the need for geometrically-complex parts produced by near-net-shape manufacturing techniques because the operations of diamond machining and finishing of densely-sintered B_4C parts are prohibitively expensive and time-consuming, if not to say inviable. Thus for example, the large front/back plates and the small side plates of body armour systems are relatively flat, so that they can be near-net-shape manufactured from dry ceramic powders by hot-pressing [6]. This is also the case for the chassis or fuselage panels of the vehicle armour systems. Other items of body armour systems, such as deltoids, shin pads, knee pads, helmets, etc., have ergonomic designs with large curvatures, and hence can be near-net-shape manufactured from colloidal ceramic suspensions by casting techniques (slip-casting, gel-casting, freeze casting, etc.) or from ceramic pastes by plastic forming processes (extrusion, injection molding, etc.), in both cases followed by pressureless sintering of the green bodies [6]. This is also the case of other items of vehicle armour systems such as nose-cone and wing/fin protections. Ceramic tribocomponents for wear applications have custom designs with specific requirements of size and geometry, and are fabricated using

different near-net-shape manufacturing techniques depending on their particular degree of shape complexity.

Fabricating dense B_4C parts is, however, very challenging in practice. This is due to the poor sinterability of B_4C [2], whose densification is intrinsically limited by the strong covalent nature of its bonding and its low self-diffusion coefficients [2,16] – a combination that imposes serious kinetics restrictions. It is for these reasons that densification of B_4C requires sintering cycles at very high temperatures ($\geq$ 2200°C) for very prolonged times (a few hours) [2]. However, even this does not completely solve the problem because the oxidic impurities (i.e., H_3BO_3 or B_2O_3) typically present in B_4C promote mass transport by surface diffusion and evaporation-condensation during the slow heating ramps applied by the conventional furnaces and hot-presses, and this favours coarsening over densification [16-19]. Consequently, sintering of B_4C is very problematic both intrinsically and extrinsically. Spark plasma sintering (SPS) uses ultra-fast sintering cycles [20,21], thus minimizing the exposure times to those temperatures at which coarsening is favoured over densification. SPS with pressure could then be used instead of hot-pressing in making B_4C parts with little curvature (i.e., geometrically simple parts) from dry powders, whereas pressureless SPS could replace conventional pressureless sintering in fabricating B_4C parts with large curvature (i.e., geometrically complex parts) from cast green bodies. Moreover, SPS could be used in combination with transient liquid-phase sintering additives to fabricate B_4C parts at smoother sintering conditions, without intergranular residual phases [22-25].

The present work was thus aimed at studying the aqueous colloidal processing of submicrometre B_4C with its coarse Ti-Al transient liquid-phase sintering additive, addressing the environmentally friendly preparation in water of both powder mixtures by freeze-drying and

complex-shape green bodies by slip-casting that could be densified by SPS (the former with pressure, and the latter without pressure). The aqueous colloidal processing of B_4C is indeed very challenging due to the innate difficulty in preparing low-viscosity concentrated suspensions of B_4C in water [26], and therefore this will be the central focus of the present study which is mostly devoted to processing and shaping aspects. The colloidal processing of B_4C in water has not been yet studied in detail, although there are some papers devoted to the dispersion of B_4C powders in order to prepare concentrated suspensions for the manufacture of bulk complex shaped parts by slip casting or gelcasting and even of laminated materials by tape casting. In those studies, several deflocculants have been used, such as ammonium polyacrylate salts [27], tetramethylammonium hydroxide [28,29], and polyethyleneimine [30,31]. Nonetheless, preliminary SPS results will also be presented as a complement to the study of the aqueous colloidal processing, which represent only a first demonstration of the densificability of both the powder mixtures and green bodies so-prepared.

2. Experimental Procedure

The starting materials were commercially available submicrometre B_4C (Grade HD 20, H.C. Starck, Germany) and micrometre Ti-Al (Alfa Aesar, Germany) powders. According to the manufacturers' specifications, the B_4C and Ti-Al powders have purities of >99 and >99.8%, respectively. In addition, characterization performed by laser scattering and He stereopycnometry indicated that the B_4C powder has a mean particle size of ~0.7 μm and an absolute density of ~2.559 g/cm^3, and that the corresponding values for the Ti-Al powder are ~38 μm and ~3.841 g/cm^3. The coarse Ti-Al particles are actually agglomerates of submicrometre primary particles of γ-TiAl (major phase), α_2-Ti_3Al (minor phase), and $TiAl_2$ (minor phase). The

B_4C and Ti-Al powders were also characterized by X-ray photoemission spectroscopy (XPS; K-Alpha, Thermo Scientific, UK), to thus examine the state of the particle surface. The procedure of aqueous colloidal processing of powders and suspensions of B_4C+Ti-Al followed the standard protocol, as will be described next.

At a first stage, the colloidal stability of the B_4C and Ti-Al powders was studied individually using dilute suspensions (0.1 g/l) with a short equilibrium time (< 10 min). To this end, systematic zeta potential measurements were made (Zetasizer Nano-ZS, Malvern, UK) as a function of pH – adjusted in the acidic or basic ranges using HCl or KOH solutions (1, 10^{-1}, or 10^{-2} M), respectively – on suspensions prepared using deionized water as suspension medium plus KCl 10^{-2} M as inert electrolyte, and sonicated for 1 min. The zeta potential measurements were made both without and with deflocculant addition. Specifically, two different commercially available polyelectrolytes were used as possible deflocculants. One is a cationic polyethylenimine (PEI; M_w ~25000; Sigma-Aldrich, USA), and the other is an anionic ammonium salt of polyacrylic acid (PAA; Duramax^{TM} D-3005, Rohm & Hams, USA). Next, at a second stage, concentrated suspensions with composition 95 vol.%B_4C+5 vol.%Ti-Al were prepared to a total solids loading of 30 vol.%, at a certain pH. The concentrated suspensions were prepared under continuous mechanical stirring with helices, using the following protocol of sequential addition. First, the desired total amount of deflocculant was incorporated into the de-ionized water (70 vol.%), followed by agitation for 5 min and sonication for 1 min. Next, the Ti-Al powder was added, followed by agitation for 5 min. Then, the B_4C powder was added gradually, after which the pH was adjusted from the natural pH to the desired value.

The resulting B_4C+5 vol.%Ti-Al concentrated suspensions were stirred for 30 min and then characterized rheologically in their as-prepared condition, and also after sonication for

different times in a min-by-min sequence with stirring for 5 min. The rheological behaviour of the suspensions was evaluated using a rheometer (MARS, Haake, Thermo, Germany) operated in controlled shear rate mode. The rheometer was configured in the double cone (cone angle of 2°)-plate geometry, and the measurement cycle of the flow curves involved a linear stretch of shear rate increase from 0 to 1000 s^{-1} in 300 s, then a plateau at 1000 s^{-1} for 60 s, and lastly a linear decrease to zero shear rate also in 300 s. The thixotropy/rheopexy was determined from the area of the flow curve's hysteresis loop, and the viscosity by direct reading at 100 and 1000 s^{-1} in the uploading stretch.

The B_4C+5 vol.%Ti-Al concentrated suspension with the best rheological behaviour was then selected to prepare both powders and green bodies. To obtain the powders, the suspension was placed in a rotary evaporator (RV10 basic, IKA, Germany) immersed in a liquid-N_2 bath, and once frozen was freeze-dried (Cryodos-50, Telstar, Spain) at -50°C and 0.3 mPa for 24 h. To obtain the green bodies, the suspension was slip-cast in bottomless plastic moulds (greased with wax) of different morphology placed on top of a flat plaster-of-Paris plate, and then was allowed to dry in air at room temperature for 48 h within the moulds. The relative density of air-dried green bodies was determined by Hg intrusion porosimetry (PoreMaster 60, Quantachrome Instruments, UK), and the microstructure was examined by scanning electron microscopy (SEM; 3600N, Hitachi, Japan).

Lastly, both the B_4C+5 vol.%Ti-Al powders and green bodies were densified by SPS (HP-D-10, FCT Systeme GmbH, Germany), the former with pressure and the latter without pressure. In particular, the powders were loaded into graphite dies (2-cm diameter) lined with graphite foil and covered by graphite blankets, and were SPS-ed in dynamic vacuum at 1900°C (as measured using an axial optical pyrometer), under 100°C/min heating, for 30 min under 75

MPa pressure. The green bodies, however, were loaded into special graphite dies designed to avoid load application and also lined with graphite foil and covered by graphite blankets, and were pressureless SPS-ed in dynamic vacuum at 1900°C (as measured using an axial optical pyrometer), under 100°C/min heating, for 60 min. Note that the SPS cycles with and without pressure are not optimized, and are therefore aimed at showing the potential densificability of both the powder mixtures and green bodies prepared here by aqueous colloidal processing. The resulting B_4C composites were ground and polished to a 1-μm finish using conventional ceramographic methods to evaluate their hardness by Vickers indentation tests (MV-1, Matsuzawa, Japan) at 9.8 N load. The B_4C composites were also intentionally broken, and the resulting fracture surfaces were observed by SEM (Quanta 3D, FEI, The Netherlands) to discriminate on the presence or absence of residual porosity. The B_4C composite fabricated by SPS with pressure was also characterized by X-ray diffractometry (XRD; D8 Advance, Bruker AXS, Germany), to identify the phases present.

3. Results and Discussion

The first step for the aqueous colloidal processing of B_4C+Ti-Al is to study the colloidal stability in water of both B_4C and Ti-Al so as to determine the appropriate conditions for their durable co-dispersion. In this context, Fig. 1 shows the evolution of the zeta potential as a function of pH for the individual dilute suspensions of B_4C and Ti-Al both without and with deflocculant (PEI or PAA). It can be seen that B_4C shows a zeta potential curve that varies smoothly with pH (i.e., with little slope and low absolute values), with its isoelectric point being located at pH~5.3. At lower or greater pHs, the zeta potential increases gradually in magnitude, reaching a value of 30 mV at pH~0.5 (estimate made by extrapolation) and of -30 mV at pH~9.5 (direct experimental measurement). At neutral pH, B_4C has a zeta potential of only -13 mV. The

isoelectric point at pH~5.3 indicates that the surface of B_4C particles is either passivated with H_3BO_3 or enriched in free carbon [26,32-34]. Indeed, the latter seems to be the likely explanation according to the XPS analysis (B 1s and C 1s core-levels) of the B_4C powder shown in Fig. 2, which indicates that the contribution of B-O bonds to the B 1s signal is very weak, whereas that of C-C bonds to the C 1s signal is very intense. Furthermore, an additional confirmation is that the isoelectric point of this B_4C powder is the same (pH~5.3) as that of a SiC nanopowder formed by SiC nanoparticles with surface enriched in carbon [35-38]. It can also be seen in Fig. 1 that the addition of only 1 wt.% PEI has two important effects on the zeta potential of B_4C. First, it markedly shifts the isoelectric point to higher pH, in particular to pH~10.5. This is because PEI is a cationic polyelectrolyte that positively charges the surface of the B_4C particles. And second, it notably increases the magnitude of the zeta potential both below and above the isoelectric point, clear evidence for electrosteric stabilization. Indeed, the zeta potential reaches values as high as 50 mV below the isoelectric point for pHs≤8.5 (thus including neutral pH). The addition of PAA has similar effects in the sense that it also shifts the isoelectric point and increases the magnitude of the zeta potential both below and above the isoelectric point, thus providing electrosteric stabilization as well. Nonetheless, unlike PEI, 0.5 wt.% PAA (*i*) shifts the isoelectric point to lower pH, in particular to pH~3.7, because it is an anionic polyelectrolyte that negatively charges the surface of the B_4C particles, and (*ii*) produces zeta potential values as high (in magnitude) as -40 mV above the isoelectric point for pHs≥5 (thus including neutral pH too).

Fig. 1 shows that the colloidal behaviour of the Ti-Al powder is qualitatively similar to that described for the B_4C powder, and therefore will be analysed more concisely. First, Ti-Al also exhibits a smooth zeta potential curve with low slope, with its isoelectric point being located at pH~4. This is essentially the isoelectric point of weakly acidic solids [39], which suggests that

the Ti-Al particles are passivated with an oxide surface. Certainly, the XPS analysis (Ti 2p and Al 2p core-levels) shown in Fig. 3 confirms this surface passivation because the contributions of Ti-O–Al-O bonds to the Ti–Al 2 p signals, respectively, are markedly more intense than the contributions of metallic Ti–Al. Second, the zeta potential also increases gradually in magnitude for pHs below or above the isoelectric point, reaching a value of 30 mV at pH<1 (estimate made by extrapolation) and of -40 mV at pH≥7.5 (direct experimental measurement). At neutral pH, Ti-Al has a zeta potential of about -33 mV. And third, the addition of PEI or PAA also provides electrosteric stabilization. Thus, with 1 wt.% PEI the isoelectric point shifts to pH~10.7, and the zeta potential reaches values as high as 45-50 mV below the isoelectric point for pHs ≤8 (thus including neutral pH). With 0.5 wt.% PAA, however, the isoelectric point shifts to pH~3, and the zeta potential reaches values as high as -40 mV above the isoelectric point for pHs≥6 (thus including neutral pH too).

The above results indicate that in principle there are two possible ways of preparing well-dispersed concentrated suspensions of B_4C+Ti-Al when one considers (*i*) that B_4C has necessarily to be deflocculated to avoid its agglomeration and to ensure the suspension's processability because it is the major solid component, (*ii*) that both B_4C and Ti-Al must have high absolute zeta potentials (i.e., at least 30 mV) with the same sign of surface charge to ensure their appropriate co-dispersion and colloidal stability, and (*iii*) that working with very acidic or basic pHs is not at all recommendable (due to health and safety concerns). With these restraints in mind, B_4C+Ti-Al suspensions can potentially be prepared in a wide range of pHs (from acidic to basic pHs) using as deflocculant (*i*) PEI together with pHs ≤9 to ensure positive zeta potentials of at least 30 mV, or (*ii*) PAA together with pHs ≥5 to ensure negative zeta potentials of at least -30 mV. Importantly, in both cases it is possible to work with water at neutral and quasi-neutral

pHs, which is very positive in terms of industrial scalability (which entails the preparation, handling, and storage of large suspension volumes, and the subsequent elimination of the corresponding liquid medium). The rheological studies of concentrated B_4C+Ti-Al suspensions will now help to elucidate which of the two deflocculants (PEI or PAA) is more recommendable, in addition to other appropriate preparation conditions (i.e., deflocculant content and sonication time).

To this end, concentrated suspensions of B_4C+5 vol.%Ti-Al were prepared as described in the experimental section at quasi-neutral pH to a total solids loading of 30 vol.% using as deflocculant 2 or 4 wt.% PEI or PAA. Note that the use of greater proportions of deflocculant in the multi-component concentrated suspensions in relation to the individual dilute suspensions is simply because in the former there is much more interaction between the particles, and therefore they are more prone to agglomeration. Interestingly, during the preparation of the concentrated suspensions it was observed that those formulated with PAA were less dispersible and much more viscous than those formulated with PEI, which already indicated that deflocculation with PEI is in principle more effective and therefore more recommendable. Indeed, as can be seen in Fig. 4, in terms of consistency, deflocculation with PAA actually led to pastes rather than suspensions. This behaviour as a paste will not prevent its use in plastic forming operations, but it is certainly undesirable in slurry shaping operations due to the poorer pouring and mould-filling performances. Fig. 5 shows the flow curves of these four B_4C+5 vol.%Ti-Al suspensions in their as-prepared condition (i.e., without sonication), measured to confirm the aforementioned visual observations. It can be seen that the suspensions prepared with PAA exhibit a very shear-thinning rheological behaviour (i.e., a plastic behaviour with a relatively high yield stress), while those prepared with PEI show a slightly shear-thinning rheological behaviour (i.e., pseudo-

plastic behaviour, without a yield point). This is indeed the flow response desirable for the wet shaping of green ceramic parts because the higher suspension viscosity under rest conditions avoids settling, thus ensuring proper storage, whereas the lower suspension viscosity under manufacturing conditions facilitates the forming of green pieces [40]. It can also be seen that the suspensions prepared with PAA are (*i*) much more viscous (i.e., viscosities slightly greater than 1 Pa·s at 100 s^{-1} and of 130-140 mPa·s at 1000 s^{-1}), and (*ii*) markedly more thixotropic/rheopexic (hysteresis loops of 15500-56000 Pa·s^{-1}) than their counterparts prepared with PEI (which have viscosities of 36-46 and 16-24 mPa·s at 100 and 1000 s^{-1}, respectively, and hysteresis loops of 10-1900 Pa·s^{-1}). This confirms quantitatively that deflocculation of the B_4C+5 vol.%Ti-Al suspensions with PEI is much more efficient, and therefore much more advisable. In addition, it is clear that the B_4C+5 vol.%Ti-Al suspensions prepared with PAA are too viscous (more than 1 Pa·s at 100 s^{-1}) to be poured appropriately, and therefore are not at all suitable for casting operations [26]. This is also the case for the aqueous suspensions of B_4C prepared using as deflocculant an anionic ammonium salt of polymethacrylic acid (i.e., Darvan C-N) or an ethanolaminic salt of citric acid (i.e., Dolapix CE 64) [26]. On the contrary, the B_4C+5 vol.%Ti-Al suspensions prepared with PEI are well suited to casting operations.

Fig. 6 shows the flow curves of the B_4C+5 vol.%Ti-Al concentrated suspensions (30 vol.% of total solids) deflocculated with 2 or 4 wt.% PEI as a function of sonication time, measured to identify which preparation conditions are more appropriate. It can be seen that they all exhibit the desirable shear-thinning rheological behaviour, with almost no thixotropy/rheopexy when sonicated. However, those prepared with 2 wt.% PEI are, for the same given sonication time, less viscous, which is a very desirable attribute. This indicates that there is a certain upper limit for the adsorption of PEI onto the surface of the B_4C and Ti-Al particles,

above which the excess of PEI stays in the water, increasing its viscosity, and thereby also the viscosity of the resulting suspensions. In addition, the sonicated suspensions prepared with 2 wt.% PEI are less time-dependent (i.e., less thixotropic/rheopexic), which is another important attribute because they are less prone to the formation/destruction of structures during the flow cycles. Finally, it can also be seen in Fig. 6 that the viscosity of the suspensions prepared with 2 or 4 wt.% PEI first decreases with increasing sonication time up to a certain time, after which the suspension viscosity increases if further sonicated. This simply reflects the excess sonication causing some re-agglomeration because the heat-induced surface activation starts to predominate over the dispersion. The optimal sonication times of the suspensions prepared with 2 and 4 wt.% PEI are 3 and 1 min, respectively. The former, however, is less viscous and less time-dependent than the latter, and therefore was the concentrated suspension chosen for freeze-drying and slip-casting.

Fig. 7 shows optical photographs of some green pieces obtained by slip-casting from the optimal B_4C+5 vol.%Ti-Al concentrated suspension, once dried in air at room temperature for 48 h. These images confirm the feasibility of using the present colloidal processing route for the near-net shaping of B_4C+Ti-Al green parts with complex geometries, as dictated simply by the mould used. In addition, the green bodies so-prepared are robust, and have good handling and storage characteristics. Fig. 8 shows SEM images of the fracture surface of these compacts in their as-cast condition. It can be seen that the green compacts have a uniform microstructure, with a good packing of particles, and without cracks, macrodefects, or density gradients. Also importantly, the as-cast pieces have a relative density (measured by Hg intrusion porosimetry) of ~60.5% (absolute density of ~1.59 g/cm^3), which is very high given that these compacts were shaped without the help of external pressure and that the limit for the random packing density of

monosized spherical particles is 64% (which nonetheless is not the present case) [41]. Indeed, these compacts are denser than others of B_4C-Ni (~59.1%) [42] and B_4C-Co (~58%) [24] prepared for a similar total solids load by aqueous slip-casting with different deflocculants, and are also denser than or equally dense as B_4C compacts prepared by non-aqueous (i.e., solutions of dodecane and Hypermer A70 dispersant) slip-casting using solid loads of 40 (~56.9%) and 45 vol.% (~60.5%) [26].

Interestingly, it can also be seen in Fig. 8 that the microstructure of the as-cast pieces contains Ti-Al particles whose size is much smaller than the ~40 μm of the Ti-Al starting powder. This suggests that the effective dispersion in water and the sonication applied during the colloidal processing broke the coarse Ti-Al starting particles, which, as mentioned above, are actually agglomerates of smaller particles (~ 1 μm). The consequence is that the Ti-Al sintering additive is better distributed over the microstructure of the B_4C compact, which is expected to facilitate the subsequent densification and to result in more uniform B_4C composites. These observations on the as-cast pieces were nonetheless validated on the freeze-dried powder mixtures. Certainly, the extensive SEM observations and EDS mappings, such as those shown by way of example in Fig. 9, also evinced the much smaller size of the Ti-Al particles in relation to their as-received condition.

To conclude, we shall also present some preliminary SPS results as a complement to the study of aqueous colloidal processing. In this regards, Fig. 10 shows SEM images of the fracture surface of the two B_4C composites, one fabricated from the freeze-dried powder mixture by SPS at 1900°C for 30 min under 75 MPa pressure, and the other from the slip-cast (green) pieces by pressureless SPS at 1900°C for 60 min. It can be seen that the former is fully dense (~2.676 g/cm^3 absolute density) and fine-grained, and that the latter is almost-fully dense (i.e., >95%) and

coarse-grained due to its longer SPS cycle. Apparently, it may seem that the SPS temperature of 1900°C used here is too high when compared with earlier work on pure B_4C [43], especially because the use of Ti-Al additives should smooth the sintering conditions. Apart from the fact that the SPS cycles are not optimized, it should be noted that different starting powders, and even the same powders processed under different methods (for example used as-received, purified, dispersed in water or in different alcohols, subjected to milling, etc.), may require different sintering conditions. It is also important to mention that care must be taken when comparing the SPS temperature reported here and in other studies because the present SPS furnace is equipped with an axial optical pyrometer (focused on a deep hole machined across the upper graphite punch), not with a radial optical pyrometer (focused close to the surface of the graphite die) as it is more usual. Also note that the advantage of using these Ti-Al additives is undisputable because a recent comparative study has demonstrated that they promote the complete densification of B_4C by transient liquid-phase sintering at SPS conditions (i.e., 1800°C (as measured using a radial optical pyrometer) for 5 min under 32 MPa pressure) at which pure B_4C does not densify (i.e., ~15.5% porosity) [23]. Beyond the SEM observations of the fracture surfaces carried out here (as needed in the context of the present study to discriminate on the presence or absence of residual porosity), the fact is that this type of B_4C composites has already been characterized microstructurally in detail elsewhere [23] by XRD, SEM, transmission electron microscopy, high-resolution electron microscopy, selected area electron diffractometry, and electron prove microanalysis demonstrating that they possess a triple-particulate microstructure formed by B_4C grains (major phase) plus TiB_2 and Al_3C_4 nanoparticles (very minor phases formed in-situ during SPS from the reaction of the molten Ti-Al intermetallics with B_4C) located at both grain boundaries and multigrain joints, with no residual Ti-Al

intermetallics. By way of example, Fig. 11 shows the XRD pattern of the B_4C composite SPS-ed with pressure demonstrating the presence of TiB_2 and Al_3C_4 also in the composites fabricated here. Interestingly, the two B_4C composites are superhard, although, due to its greater densification, the one fabricated from the powder mixture by SPS with pressure is slightly harder (i.e., 34±1 GPa) than the one fabricated from the slip-cast (green) pieces by SPS without pressure (i.e., 32±1 GPa). These hardness values are consistent with the expected value (~33±1 GPa) for fully dense and almost-fully dense B_4C composites prepared with 5 vol.% Ti-Al (i.e., with ~7.33 wt.% Ti-Al) [23]. Finally, it should be mentioned that, although the SPS cycles with and without pressure have yet to be conveniently optimized, these preliminary SPS tests at least demonstrate the usefulness of the present route of aqueous colloidal processing for the future eco-friendly fabrication of advanced B_4C composites (once the SPS cycles have been appropriately adjusted in subsequent studies).

4. Concluding Remarks

We have described a procedure of aqueous colloidal processing for the environmentally friendly preparation of well dispersed concentrated suspensions, and therefrom powder mixtures, of commercially available powders of submicrometre B_4C (~0.6 μm) with coarse Ti-Al (~40 μm) as transient liquid-phase sintering additive. It was shown that B_4C has little colloidal stability in water, requiring very basic pH (i.e., pH>10) for its individual dispersion. Ti-Al has greater colloidal stability than B_4C, requiring quasi-neutral pH or above (i.e., pH>7.5) for its individual dispersion. The addition of cationic (i.e., PEI) or anionic (i.e., PAA) deflocculants simultaneously improves the colloidal stability of both B_4C and Ti-Al, making their co-dispersion possible at neutral pH ($pH \leq 9$ and $pH \geq 5$ when using PEI and PAA, respectively). It was also shown that, although the concentrated suspensions (i.e., 30 vol.% total solids) can be

deflocculated with PEI or PAA, the former are less viscous and thixotropic/rheopexic than the latter and have the desirable shear-thinning rheological behaviour, being therefore preferable for obtaining both powder mixtures by freeze-drying and green pieces by slip-casting. Finally, preliminary SPS tests demonstrated the feasibility of fabricating superhard B_4C composites from these powder mixtures by conventional SPS with pressure or from the slip-cast (green) pieces by pressureless SPS.

Acknowledgements. This work was supported by the Ministerio de Economía y Competitividad (Government of Spain) and FEDER Funds under the Grants nº MAT2016-76638-R and MAT2015-67586-C3-2-R. Financial support from the Junta de Extremadura under the Grant nº GR15078, also co-financed with FEDER Funds, is gratefully acknowledged as well. Cristina Ojalvo thanks the Junta de Extremadura for the funding provided under her PhD Grant nº PD16027.

References

1. F. Thevenot, Boron carbide - a comprehensive review, J. Eur. Ceram. Soc. 6 [4] (1990) 205–225.
2. A.K. Suri, C. Subramanian, J.K. Sonber, T.S.R.-Ch. Murthy, Synthesis and consolidation of boron carbide: a review, Int. Mater. Rev. 55 [1] (2010) 4–40.
3. V. Domnich, S. Reynaud, R.A. Haber, M. Chhowalla, Boron carbide: structure, properties, and stability under stress, J. Am. Ceram. Soc. 94 [11] (2011) 3605–3628.
4. M. Chen, J.W. McCauley, K.J. Hemker, Shock-induced localized amorphization in boron carbide, Science 299 (2003) 1563–1566.
5. H. Way, N.F. Particle, Media-milled nanoparticles boosts ceramic armor, Am. Ceram. Soc. Bull. 87 [5] (2008) 20–24.
6. S. Leo, C. Tallon, G.V. Franks, Near-net-shaping methods for ceramic elements of (body) armor systems, J. Am. Ceram. Soc. 97 [10] (2014) 3013–3033.
7. D. Hallam, A. Heaton, B. James, P. Smith, J. Yeomans, The correlation of indentation behaviour with ballistic performance for spark plasma sintered armour ceramics, J. Eur. Ceram. Soc. 35 [8] (2015) 2243–2252.
8. S. Hayun, Reaction-bonded boron carbide for lightweight armor: the interrelationship between processing, microstructure, and mechanical properties, Am. Ceram. Soc. Bull. 96 [6] (2017) 22–29.
9. K.A. Schwetz, L.S. Sigl, J. Greim, H. Knoch, Wear of boron carbide ceramics by abrasive waterjets, Wear 181–183 (Part 1) (1995) 148–155.
10. J. Deng, Erosion wear of boron carbide ceramics nozzles by abrasive air-jets, Mater. Sci. Eng. A 408 (1–2) (2005) 227–233.

11. J.E. Zorzi, C.A. Perottoni, J.A.H. da Jornada, Hardness and wear resistance of B_4C ceramics prepared with several additives, Mater. Lett. 59 (23) (2005) 2932–2935.

12. W. Lin, N. Feng, L. He, Wear properties of reaction sintered B_4C composites, Adv. Mater. Res. 152–153 (2011) 883–886.

13. S. Junlong, L. Changxia, T. Jin, F. Baofu, Erosion behavior of B_4C based ceramic nozzles by abrasive air-jet, Ceram. Int. 38 (8) (2012) 6599–6605.

14. B.M. Moshtaghioun, D. Gómez-García, A. Domínguez-Rodríguez, R.I. Todd, Abrasive wear rate of boron carbide ceramics: influence of microstructural and mechanical aspects on their tribological response, J. Eur. Ceram. Soc. 36 [16] (2016) 3925–3928.

15. A.L. Ortiz, V.M. Candelario, O. Borrero-López, F. Guiberteau, Sliding-wear resistance of pure near fully-dense B_4C under lubrication with water, diesel fuel, and paraffin oil, J. Eur. Ceram. Soc. 38 [4] (2018) 1158–1163.

16. S.L. Dole, S. Prochazka, R.H. Doremus, Microstructural coarsening during sintering of boron carbide, J. Am. Ceram. Soc. 72 [6] (1989) 958–966.

17. S.L. Dole, S. Prochazka, Densification and microstructure development in boron carbide, Ceram. Eng. Sci. Proc. 6 [7-8] (1985) 1151–1160.

18. S. Prochazka, S.L. Dole, C.I. Hejna, Abnormal grain growth and microcracking in boron carbide, J. Am. Ceram. Soc. 68 [9] (1985) c235–c236.

19. H. Lee, R.F. Speyer, Pressureless sintering of boron carbide, J. Am. Ceram. Soc. 86 [9] (2003) 1468–1473.

20. Z.A. Munir, U. Anselmi-Tamburini, M. Ohyanagi, The effect of electric field and pressure on the synthesis and consolidation of materials: a review of the spark plasma sintering method, J. Mat. Sci. 41 [3] (2006) 763–777.

21. Z.A. Munir, D.V. Quach, Electric current activation of sintering: a review of the pulsed electric current sintering process, J. Am. Ceram. Soc. 94 [1] (2011) 1–19.

22. S. Kumar, K. Sairam,J.K. Sonber, T.S.R.Ch. Murthy, V. Reddy, G.V.S. Nageswara Rao, T. Srinivasa Rao, Hot-pressing of $MoSi_2$ reinforced B_4C composites, Ceram. Inter. 40 [10 Part B] (2014) 16099–16105.

23. W. Ji, R.I. Todd, W. Wang, H. Wang, J. Zhang, Z. Fu, Transient liquid phase spark plasma sintering of B_4C-based ceramics using Ti-Al intermetallics as sintering aid, J. Eur. Ceram. Soc. 36 [10] (2016) 2419–2426.

24. A.L. Ortiz, V.M. Candelario, R. Moreno, F. Guiberteau, Near-net shape manufacture of B_4C–Co and ZrC–Co composites by slip casting and pressureless sintering, J. Eur. Ceram. Soc. 37 [15] (2017) 4577–4584.

25. C. Ojalvo, F. Guiberteau, A.L. Ortiz, Fabricating toughened super-hard B_4C composites at lower temperature by transient liquid-phase assisted spark plasma sintering with $MoSi_2$ additives, J. Eur. Ceram. Soc. 39 [9] (2019) 2862–2873.

26. S. Leo, C. Tallon, G.V. Franks, Aqueous and nonaqueous colloidal processing of difficult-to-densify ceramics: suspension rheology and particle packing, J. Am. Ceram. Soc. 97 [12] (2014) 3807–3817.

27. M. Dawes, S, Blackburn, R. Greenwood, S. Charles, A zeta potential and rheology study using electroacoustic spectroscopy on aqueous boron carbide suspensions, Ceram. Int. 44 [18] (2018) 23208–23214.

28. J. Zhang, D. Jiang, Q. Lin, Aqueous processing of boron carbide powders, J. Ceram. Soc. Japan 116 [6] (2008) 681–684.

29. Z. Luo, Z. Lv, D. Jiang, J. Zhang, Z. Chen, Z. Huang, Aqueous tape casting of boron carbide ceramic, Ceram. Int. 39 [2] (2013) 2123–2126.

30. X.J. Zeng, W.L. Liu, Aqueous tape casting of B_4C ceramics, Adv. Appl. Ceram. 115 [4] (2016) 224–228.

31. A. Diaz-Cano, R.W. Trice, J.P. Youngblood, Stabilization of highly-loaded boron carbide aqueous suspensions, Ceram. Int. 43 [12] (2017) 8572–8578.

32. P.D. Williams, D.D. Hawn, Aqueous dispersion and slip casting of boron carbide powder: effect of pH and oxygen content, J. Am. Ceram. Soc. 74 [7] (1991) 1614–1618.

33. I. Varga, F. Csempesz, G.Záray, Effect of pH of aqueous ceramic suspensions on colloidal stability and precision of analytical measurements using slurry nebulization inductively coupled plasma atomic emission spectrometry, Spectrochim. Acta B 51 [2] (1996) 253–259.

34. X. Li, D. Jiang, J. Zhang, Q. Lin, Z. Chen, Z. Huang, The dispersion of boron carbide powder in aqueous media, J. Eur. Ceram. Soc. 33 [10] (2013) 1655–1663.

35. V.M. Candelario, R. Moreno, A.L. Ortiz, Carbon nanotubes prevent the coagulation at high shear rates of aqueous suspensions of equiaxed ceramic nanoparticles, J. Eur. Ceram. Soc. 34 [3] (2014) 555–563.

36. V.M. Candelario, R. Moreno, Z. Shen, A.L. Ortiz, Aqueous colloidal processing of nano-SiC and its nano-$Y_3Al_5O_{12}$ liquid-phase sintering additives with carbon nanotubes, J. Eur. Ceram. Soc. 35 [13] (2015) 3363–3368.

37. V.M. Candelario, R. Moreno, R.I. Todd, A.L. Ortiz, Liquid-phase assisted flash sintering of SiC from powder mixtures prepared by aqueous colloidal processing, J. Eur. Ceram. Soc. 37 [2] (2017) 485–498.

38. V.M. Candelario, R. Moreno, F. Guiberteau, A.L. Ortiz, Fabricating eco-friendly nanocomposites of SiC with morphologically-different nano-carbonaceous phases, J. Eur. Ceram. Soc. 38 [11] (2018) 3735–3741.

39. M. Kosmulski, Isoelectric points and points of zero charge of metal (hydr)oxides: 50 years after Parks' review, Adv. Colloid. Interface Sci. 238 (2016) 1–61.

40. R. Moreno, Reología de suspensiones cerámicas, Consejo Superior de Investigaciones Científicas, Madrid, Spain (2005).

41. R.M. German, Sintering theory and practice, Wiley, New York, USA (1996).

42. F. Rodríguez-Rojas, R. Moreno, F. Guiberteau, A.L. Ortiz, Aqueous colloidal processing of near-net shape B_4C-Ni cermet compacts, J. Eur. Ceram. Soc. 36 [8] (2016) 1915–1921.

43. B.M. Moshtaghioun, F.L. Cumbrera-Hernández, D. Gómez-García, S. Bernardi-Martín, A. Domínguez-Rodríguez, A. Monshi, M.H. Abbasi, Effect of spark plasma sintering parameters on microstructure and room-temperature hardness and toughness of fine-grained boron carbide (B_4C), J. Eur. Ceram. Soc. 33 [2] (2013) 361–369.

Figure Captions

Figure 1. Dependence on pH and deflocculant content (PEI and PAA) of the zeta potential for the individual dilute suspensions of B_4C and Ti-Al, as indicated. Dots are the experimental data, and the lines are guides for the eye. The grey stripe denotes the zone of low colloidal stability.

Figure 2. XPS spectra of the as-received B_4C powder showing the (A) B 1s and (B) C 1s core-levels. Peak assignations are included.

Figure 3. XPS spectra of the as-received Ti-Al powder showing the (A) Ti 2p and (B) Al 2p core-levels. Peak assignations are included.

Figure 4. Optical photographs taken during the preparation of the B_4C+5 vol.%Ti-Al concentrated suspensions with (A) 2 wt.% PAA, (B) 4 wt.% PAA, (C) 2 wt.% PEI, and (C) 4 wt.% PEI. Note that the slurries in (A) and (B) are very thick and resemble pastes, to such an extent that the helices used for the mechanical agitation left a residual imprint. The slurries in (C) and (D) are, however, very thin and resemble suspensions.

Figure 5. Flow curves of the B_4C+5 vol.%Ti-Al concentrated suspensions prepared without sonication using as deflocculant 2 or 4 wt.% PEI or PAA. The arrows indicate, where applicable, the uploading and downloading stretches of the flow curves.

Figure 6. Flow curves of the B_4C+5 vol.%Ti-Al concentrated suspensions prepared with (A) 2 or (B) 4 wt.% PEI as a function of sonication time. Sonication was not prolonged further once the flow curve worsened. The number at the right of each curve denotes the sonication time. The arrows indicate, where applicable, the uploading and downloading stretches of the flow curves.

Figure 7. Photographs of various green pieces obtained by slip-casting from the B_4C+5 vol.%Ti-Al concentrated suspension prepared with 2 wt.% PEI and sonicated for 3 min. Photographs were taken after drying in air at room temperature for 48 h.

Figure 8. Representative SEM image (fracture surface) of a green microstructure of the B_4C+5 vol.%Ti-Al compacts in Fig. 8. The insets at the top-left and top-right corners are the slip-cast body and a higher-magnification SEM image, respectively.

Figure 9. (A) Representative SEM image of a powder mixture obtained by freeze-drying the B_4C+5 vol.%Ti-Al concentrated suspension prepared with 2 wt.% PEI and sonicated for 3 min, and the corresponding elemental compositional maps of (B) C, (C) Ti, and (D) Al.

Figure 10. Representative SEM micrographs of the fracture surface of the B_4C composites fabricated by SPS at 1900°C (A) for 30 min under 75 MPa pressure from the powder mixtures, and (B) for 60 min without pressure from the slip-cast pieces.

Figure 11. XRD pattern of the B_4C composite fabricated by SPS at 1900°C for 30 min under 75 MPa pressure from the powder mixtures. Peak assignations are included. Note that a logarithmic scale has been used in the intensity axis to facilitate the observation of the weak peaks from C, TiB_2, and Al_4C_3 (which are less intense than the B_4C peaks by various orders of magnitude).

Figure

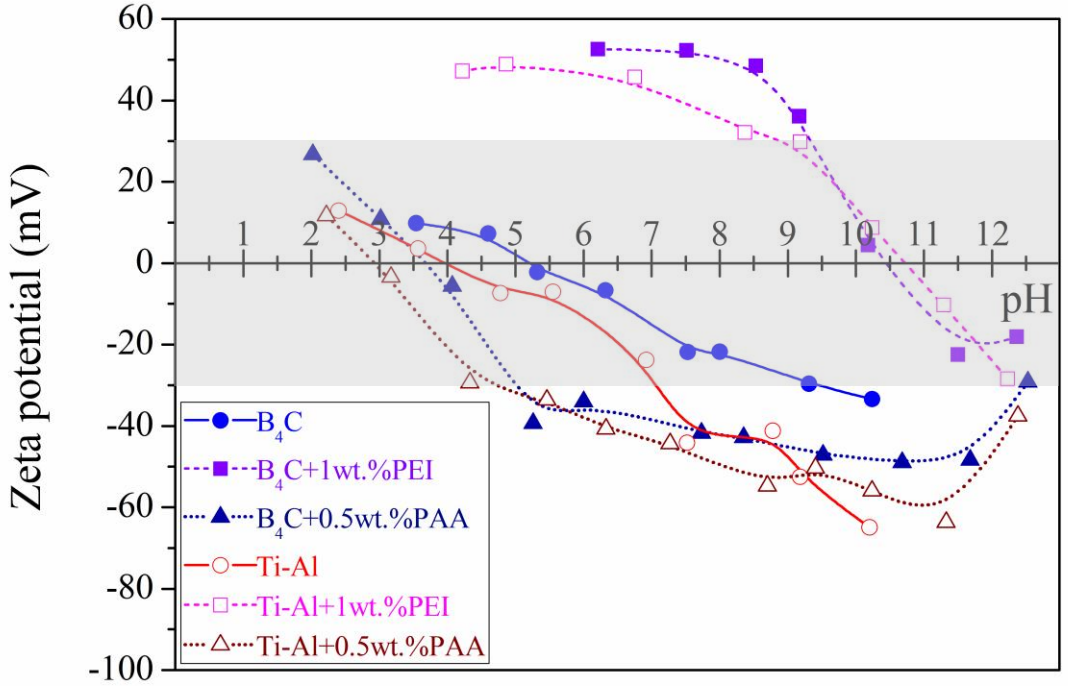

Ojalvo *et al.*
Figure 1

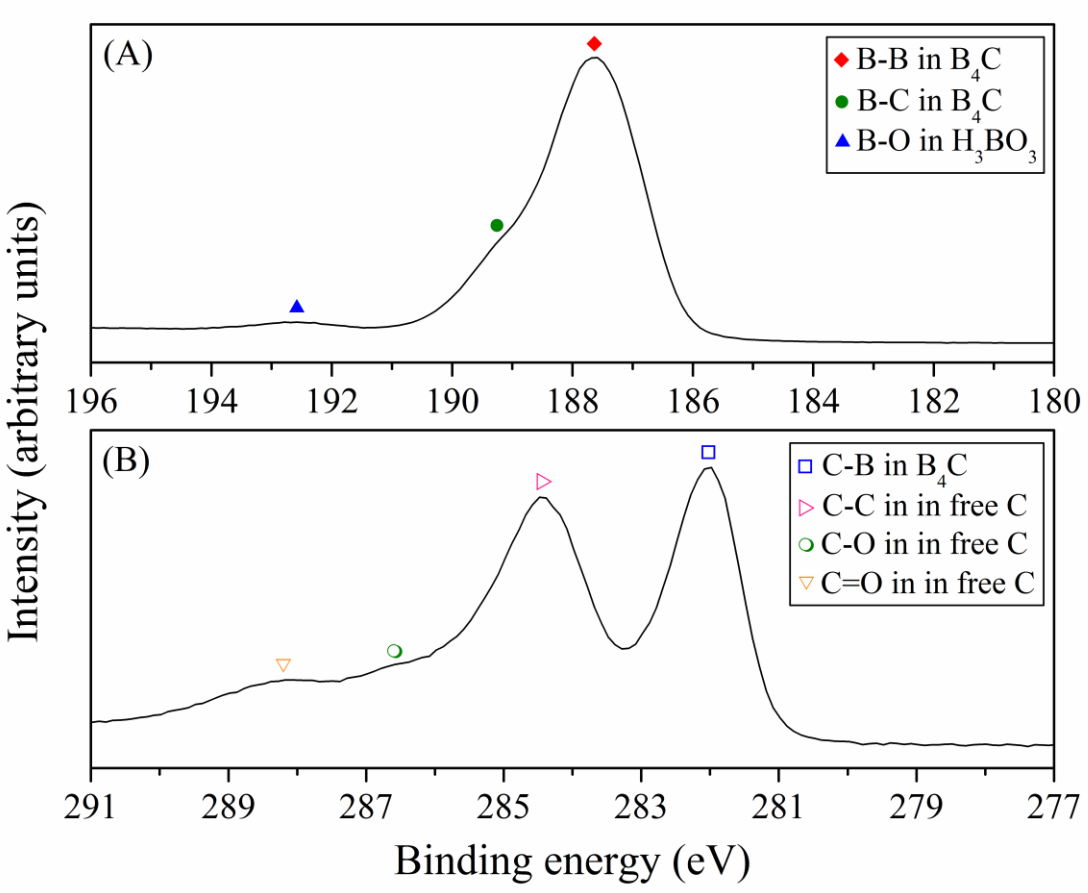

Ojalvo *et al.*
Figure 2

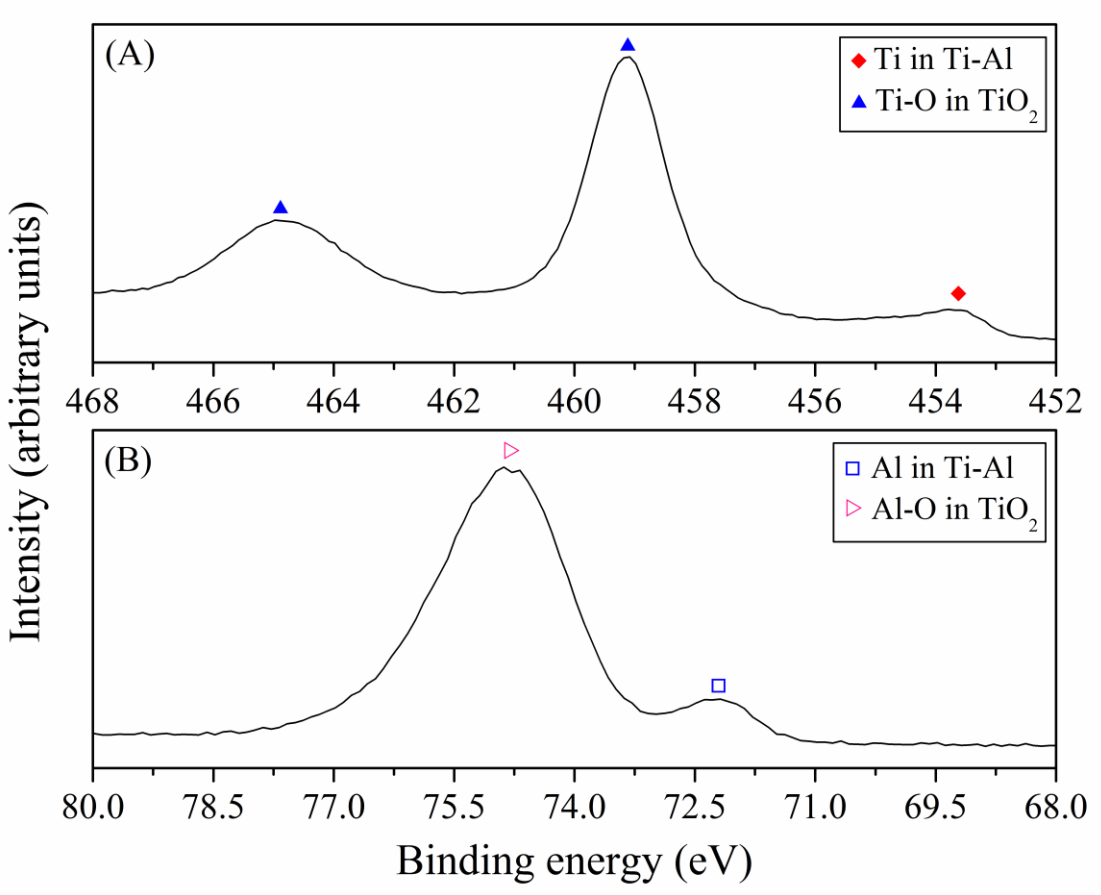

Ojalvo *et al.*
Figure 3

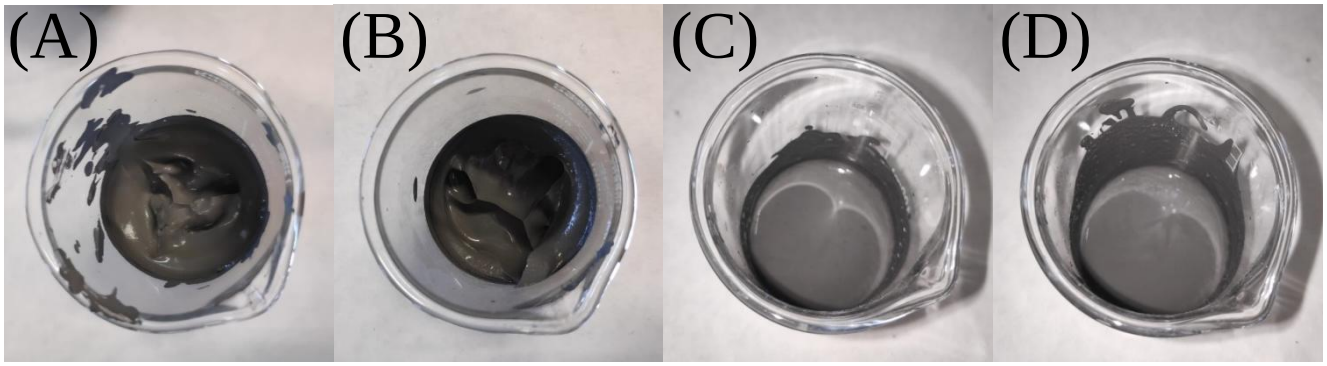

Ojalvo *et al.*
Figure 4

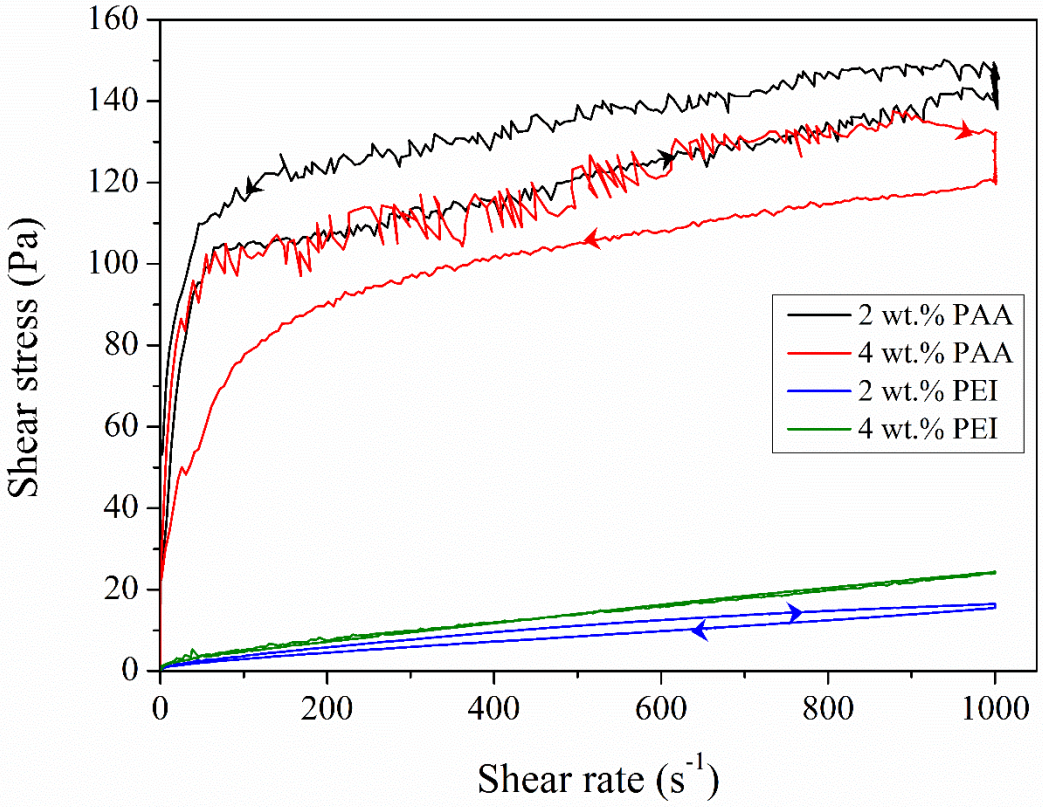

Ojalvo *et al.*
Figure 5

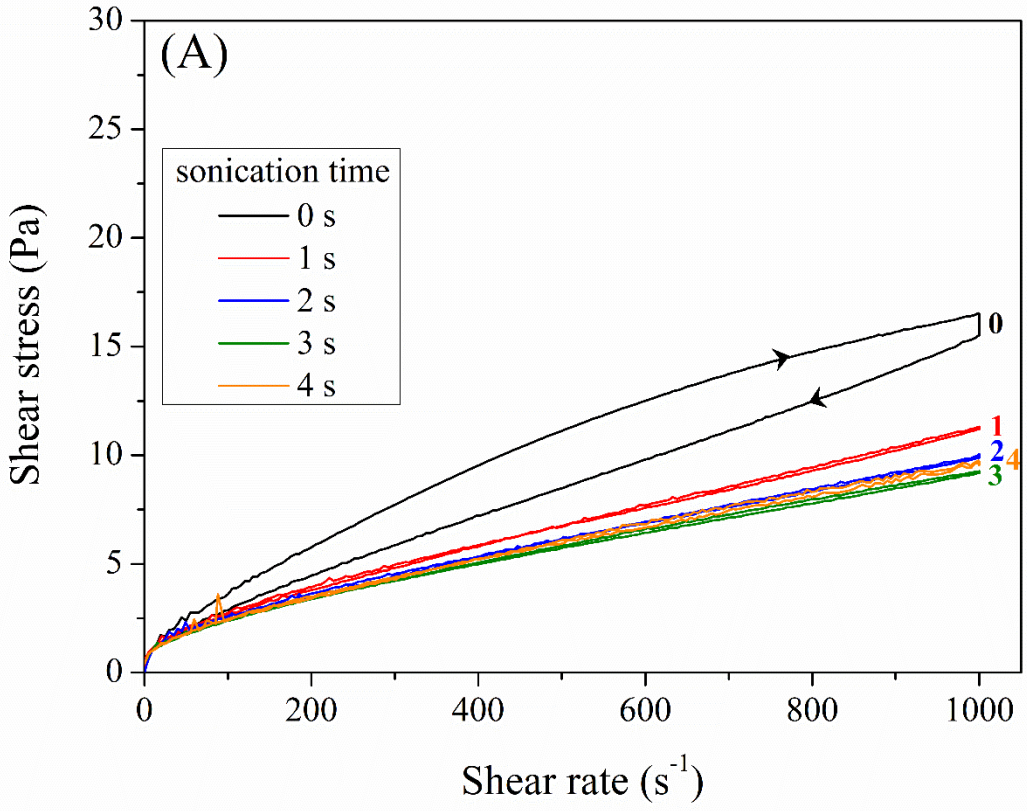

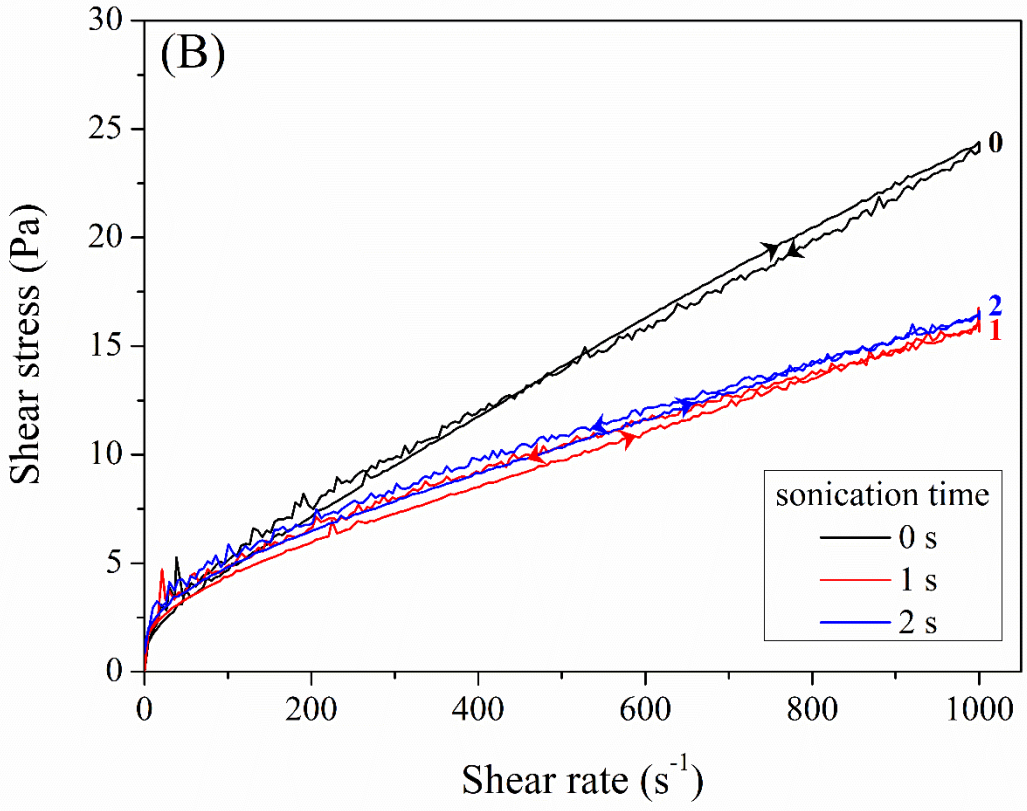

Ojalvo *et al.*
Figure 6

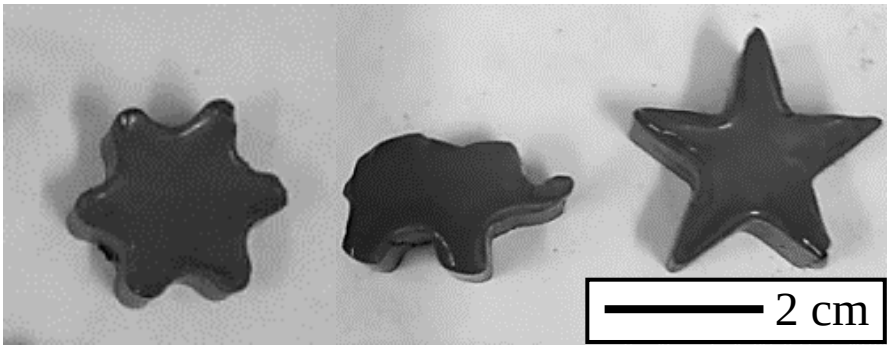

Ojalvo *et al.*
Figure 7

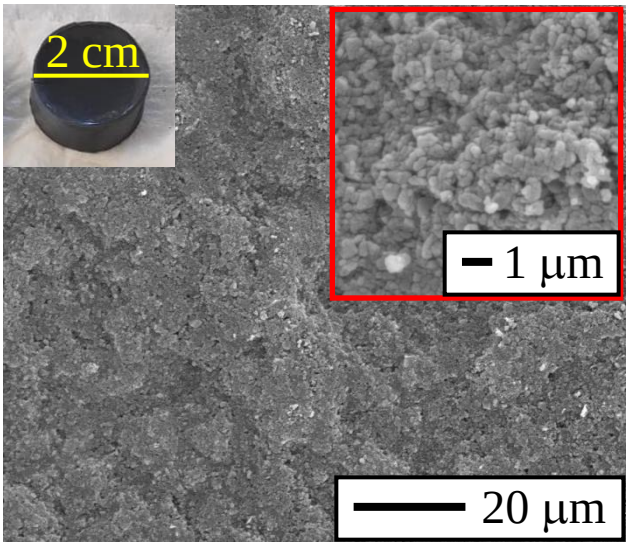

Ojalvo *et al.*
Figure 8

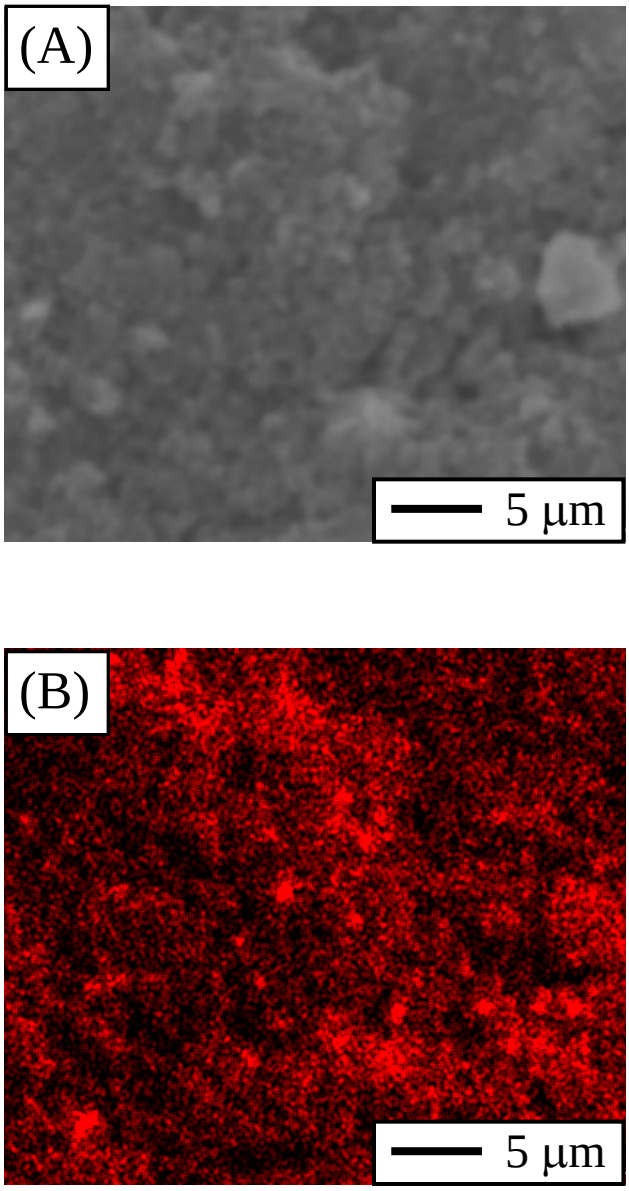

Ojalvo *et al.*
Figure 9

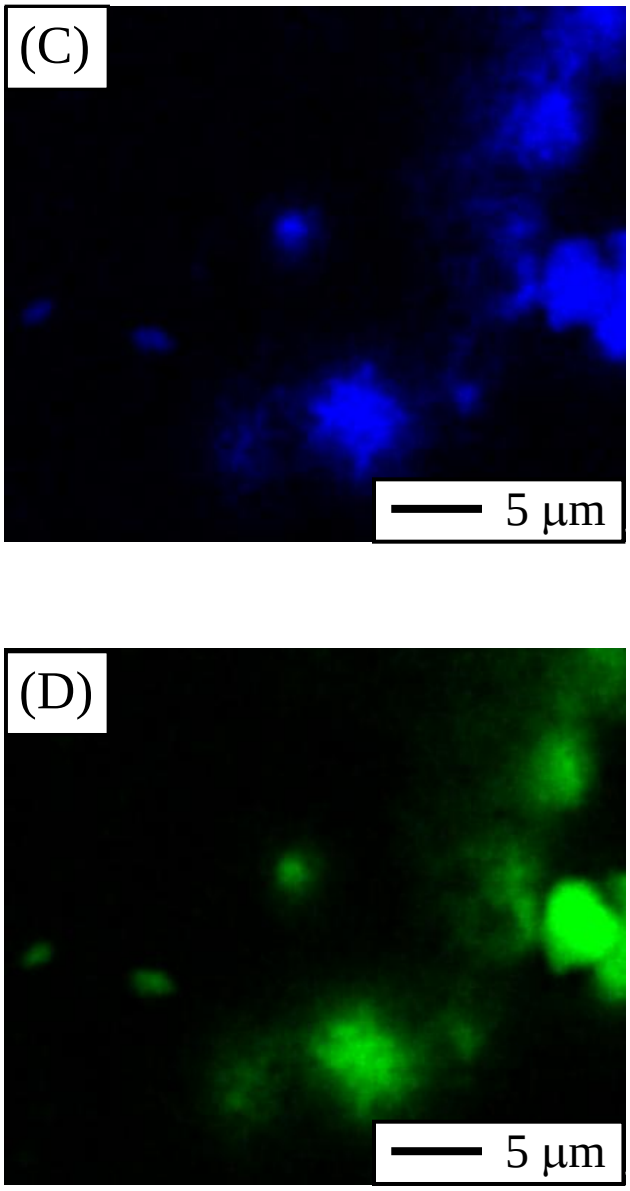

Ojalvo *et al.*
Figure 9

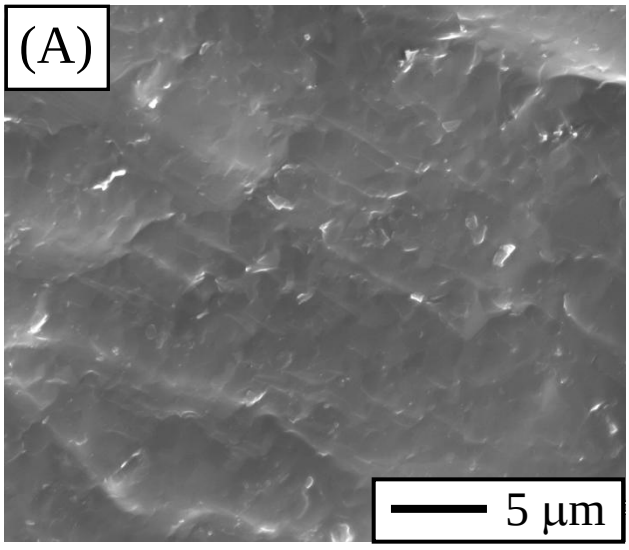

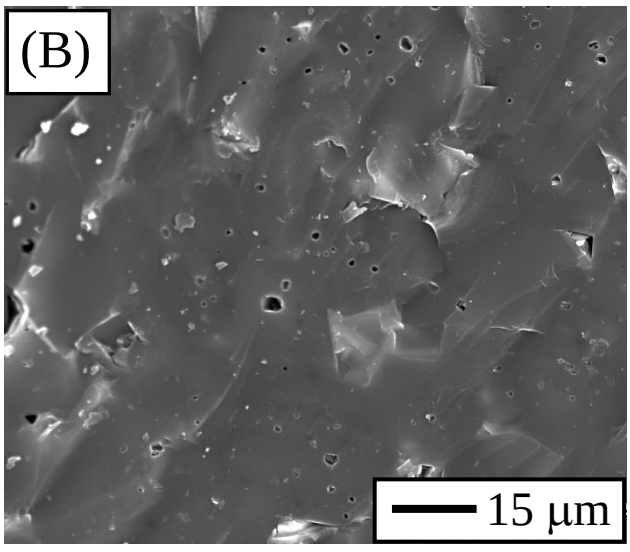

Ojalvo *et al.*
Figure 10

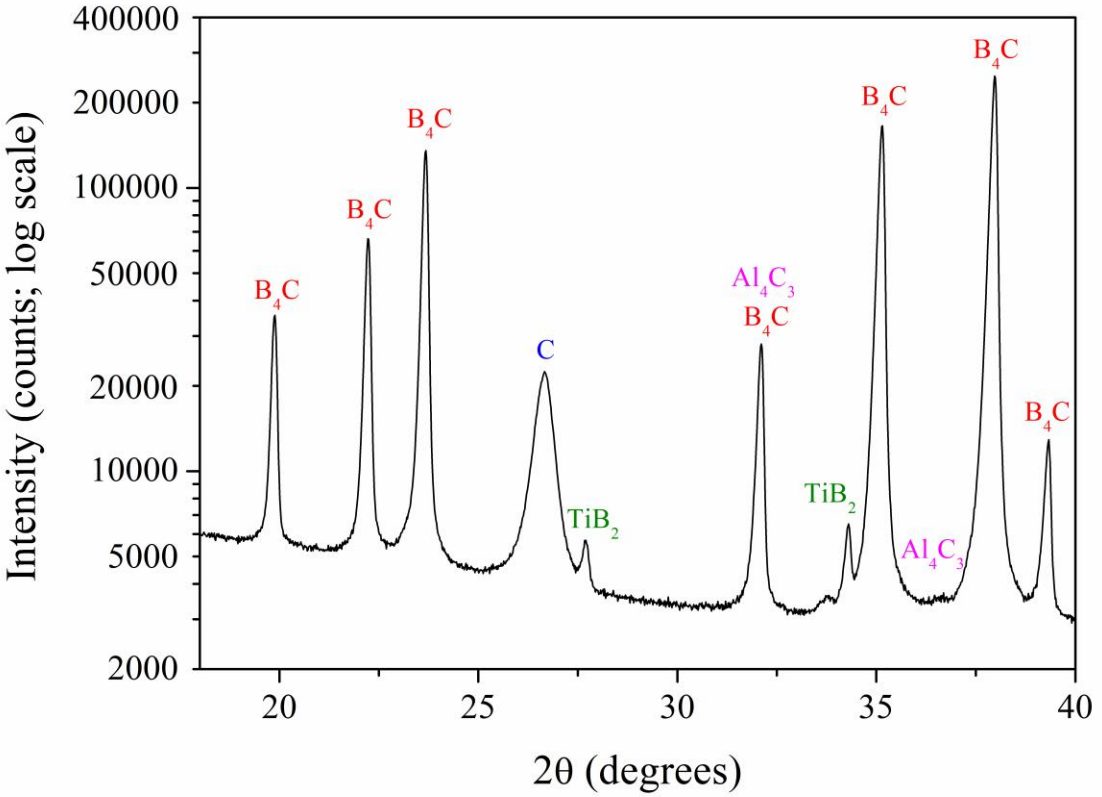

Ojalvo *et al.*
Figure 11

Figure Captions

Figure 1. Dependence on pH and deflocculant content (PEI and PAA) of the zeta potential for the individual dilute suspensions of B_4C and Ti-Al, as indicated. Dots are the experimental data, and the lines are guides for the eye. The grey stripe denotes the zone of low colloidal stability.

Figure 2. XPS spectra of the as-received B_4C powder showing the (A) B 1s and (B) C 1s core-levels. Peak assignations are included.

Figure 3. XPS spectra of the as-received Ti-Al powder showing the (A) Ti 2p and (B) Al 2p core-levels. Peak assignations are included.

Figure 4. Optical photographs taken during the preparation of the B_4C+5 vol.%Ti-Al concentrated suspensions with (A) 2 wt.% PAA, (B) 4 wt.% PAA, (C) 2 wt.% PEI, and (C) 4 wt.% PEI. Note that the slurries in (A) and (B) are very thick and resemble pastes, to such an extent that the helices used for the mechanical agitation left a residual imprint. The slurries in (C) and (D) are, however, very thin and resemble suspensions.

Figure 5. Flow curves of the B_4C+5 vol.%Ti-Al concentrated suspensions prepared without sonication using as deflocculant 2 or 4 wt.% PEI or PAA. The arrows indicate, where applicable, the uploading and downloading stretches of the flow curves.

Figure 6. Flow curves of the B_4C+5 vol.%Ti-Al concentrated suspensions prepared with (A) 2 or (B) 4 wt.% PEI as a function of sonication time. Sonication was not prolonged further once the flow curve worsened. The number at the right of each curve denotes the sonication time. The arrows indicate, where applicable, the uploading and downloading stretches of the flow curves.

Figure 7. Photographs of various green pieces obtained by slip-casting from the B_4C+5 vol.%Ti-Al concentrated suspension prepared with 2 wt.% PEI and sonicated for 3 min. Photographs were taken after drying in air at room temperature for 48 h.

Figure 8. Representative SEM image (fracture surface) of a green microstructure of the B_4C+5 vol.%Ti-Al compacts in Fig. 8. The insets at the top-left and top-right corners are the slip-cast body and a higher-magnification SEM image, respectively.

Figure 9. (A) Representative SEM image of a powder mixture obtained by freeze-drying the B_4C+5 vol.%Ti-Al concentrated suspension prepared with 2 wt.% PEI and sonicated for 3 min, and the corresponding elemental compositional maps of (B) C, (C) Ti, and (D) Al.

Figure 10. Representative SEM micrographs of the fracture surface of the B_4C composites fabricated by SPS at 1900°C (A) for 30 min under 75 MPa pressure from the powder mixtures, and (B) for 60 min without pressure from the slip-cast pieces.

Figure 11. XRD pattern of the B_4C composite fabricated by SPS at 1900°C for 30 min under 75 MPa pressure from the powder mixtures. Peak assignations are included. Note that a logarithmic scale has been used in the intensity axis to facilitate the observation of the weak peaks from C, TiB_2, and Al_4C_3 (which are less intense than the B_4C peaks by various orders of magnitude).

***Summary of Novel Conclusions**

- A route of aqueous colloidal processing of submicrometre B_4C powder (~0.6 μm) with coarse Ti-Al powder (~40 μm) is presented and optimized.
- Concentrated suspensions of B_4C+Ti-Al are prepared for the near-net shape manufacture of B_4C composites by slip casting and pressureless spark plasma sintering.
- Powder mixtures of B_4C+Ti-Al are prepared for the near-net shape manufacture of B_4C composites by conventional spark plasma sintering.
- Superhard B_4C composites are obtained in an environmentally friendly manner.